Adsorption mechanism of an antimicrobial peptide on carbonaceous surfaces: A molecular dynamics study

Danilo Roccatano,[1,a)] Edita Sarukhanyan,[2,b)] and Ronen Zangi[3,4]
[1]*School of Mathematics and Physics, University of Lincoln, Brayford Pool, Lincoln LN6 7TS, United Kingdom*
[2]*School of Engineering and Science, Jacobs University Bremen, Campus Ring 1, 28759 Bremen, Germany*
[3]*Polymat and Department of Organic Chemistry I, University of the Basque Country UPV/EHU, Avenida de Tolosa 72, 20018 San Sebastian, Spain*
[4]*IKERBASQUE, Basque Foundation for Science, Maria Diaz de Haro 3, 48013 Bilbao, Spain*

(Received 5 November 2016; accepted 12 January 2017; published online 15 February 2017)

Peptides are versatile molecules with applications spanning from biotechnology to nanomedicine. They exhibit a good capability to unbundle carbon nanotubes (CNT) by improving their solubility in water. Furthermore, they are a powerful drug delivery system since they can easily be uptaken by living cells, and their high surface-to-volume ratio facilitates the adsorption of molecules of different natures. Therefore, understanding the interaction mechanism between peptides and CNT is important for designing novel therapeutical agents. In this paper, the mechanisms of the adsorption of antimicrobial peptide Cecropin A–Magainin 2 (CA-MA) on a graphene nanosheet (GNS) and on an ultra-short single-walled CNT are characterized using molecular dynamics simulations. The results show that the peptide coats both GNS and CNT surfaces through preferential contacts with aromatic side chains. The peptide packs compactly on the carbon surfaces where the polar and functionalizable Lys side chains protrude into the bulk solvent. It is shown that the adsorption is strongly correlated to the loss of the peptide helical structure. In the case of the CNT, the outer surface is significantly more accessible for adsorption. Nevertheless when the outer surface is already covered by other peptides, a spontaneous diffusion, via the amidated C-terminus into the interior of the CNT, was observed within 150 ns of simulation time. We found that this spontaneous insertion into the CNT interior can be controlled by the polarity of the entrance rim. For the positively charged CA-MA peptide studied, hydrogenated and fluorinated rims, respectively, hinder and promote the insertion. *Published by AIP Publishing.* [http://dx.doi.org/10.1063/1.4975689]

INTRODUCTION

The allotriomorphic properties of carbon atoms result in nanomaterials of different shapes and surface curvatures such as the cylindrical hollow carbon nanotubes (CNTs) and the planar graphene nano-sheets (GNSs). These materials exhibit many unique properties, which makes them attractive for applications in the emerging field of nanomedicine. It has been shown that CNTs can act as ion channel blockers,[1] artificial muscles,[2] and sensors,[3,4] as well as drug-delivery vehicles.[5] In addition, grafting these materials with anchors that possess tailored properties can create functional surfaces for specific applications. For example, it is possible to generate antibacterial surfaces for medical use by coating the surface with antimicrobial peptides (AMPs). These AMPs are broadly distributed in different types of organisms playing an important role in both the host defense system and the innate immunity.[6–10] However, one of the major obstacles to the use of CNTs and GNS in living systems is their poor solubility in water. In fact, they usually form insoluble aggregates (bundles) which can evoke cytotoxic effects.[11–15] Covalent[16,17] or non-covalent[18–20] surface modifications with biocompatible materials can help to solve this problem. For this reason, great effort is devoted to understand the adsorption mechanism of biomolecules, such as peptides[21] and nucleic acids,[22] to carbon-based nanomaterial surfaces. When covered with peptides, these carbon-based proteinaceous materials have the advantage that their properties can be easily designed by incorporating different amino acids into the adsorbing peptides. In addition, AMPs[23–25] are potential alternatives to traditional antibiotics in the battle against new drug resistant bacteria strains and cancers.[26,27] Several structure-function studies of different natural and artificial peptides have been performed to understand their antimicrobial and anticancer properties.[24,28,29]

Two well-studied AMPs are the Cecropin A (CA) and the Magainin 2 (MA). CA is a 37 amino acid antimicrobial peptide found in the hemolymph of *Hyalophora cecropia* pupae[6,23,25,30–33] and MA is a 23 amino acid long peptide extracted from the skin of the African clawed frog, *Xenopus laevis*.[6,9,34–36] Both CA and MA have strong lytic activities against Gram-positive and Gram-negative bacteria without toxic effects to eukaryotic cells, such as human erythrocytes.[6,9,30,34] Among the different hybrid peptides derived from CA and MA peptides, the one composed from

[a)]Author to whom correspondence should be addressed. Electronic mail: droccatano@lincoln.ac.uk. Tel.: +44 1522 835868.
[b)]Current address: Department of Bioinformatics, Biozentrum, Universität Würzburg, Am Hubland, D-97074 Wuerzburg, Germany.

residues 1-8 of CA and residues 1-12 of MA, resulting in the amino acid sequence KWKLFKKI-GIGKFLHSAKKF-$CONH_2$, was found to exhibit better antibacterial and antitumor activities compared with those of the starting peptides.[23–25,28,29] This CA-MA chimeric peptide can have potential use in preventing bacterial contamination of composite nanomaterials or in drug delivery systems using CNT as drug releasing nanocontainer or vectors.

For all these applications, it is important to understand the mechanism of adsorption of the molecule on the surface and how the presence of solid surfaces affects the peptide conformation. The structure of the CA-MA peptide in water solution without carboneous nanomaterials has been investigated by Nuclear Magnetic Resonance (NMR) spectroscopy and circular dichroism[24,37] and recently in our group using molecular dynamics (MD) simulations.[38] MD simulation is one of the most powerful methods to investigate with full atomic details the structure and dynamics of biomolecules. Although several experimental and theoretical studies on the interaction of peptides with CNT were reported in the literature,[21,39–45] none had targeted the interaction of the CA-MA peptide with CNT or GNS.

In this paper, we used CA-MA as a model peptide to study by computer simulations the binding mechanism of peptides to carboneous nanomaterials. In particular, we performed extensive MD simulations of the peptide in aqueous solutions in the presence of either a single-walled CNT (SWCNT) (10, 10) or a GNS of the same surface area as the SWCNT. The binding and absorption mechanisms of the peptides were studied at different peptide concentrations. We analysed the spontaneous diffusion of the peptide into the SWCNT and the effect of atomic partial charges at the SWCNT edges on the peptide-nanotube interaction.

METHODS

The coordinates of the hybrid peptide Cecropin A–Magainin 2 (CA-MA) were taken from the Protein Data Bank (PDB), entry code 1D9J.[37] Its NMR structure and amino acid sequence are shown in Figure 1. The dimension of the graphene sheets considered in this study was around 6.2 × 4.3 nm^2. The SWCNTs were characterized by chiral indices of m = 10 and n = 10, resulting in a diameter of approximately 1.3 nm, and a length of 6 nm. The –CH groups at the edges of the GNS and SWCNT were modeled as united-atom sites each carrying zero charge unless otherwise indicated. To model the non-bonded interactions within the CNT or GNS, we used the following carbon–carbon Lennard-Jones (LJ) parameters: ε_{cc} = 0.4396 kJ mol^{-1} and σ_{cc} = 0.3851 nm.[46] The interactions of these carbon-based materials with water were represented by the carbon–water LJ parameters ε_{co} = 0.392 kJ mol^{-1} and σ_{co} = 0.319 nm.[47] The same parameters were adopted for the united atom sites.

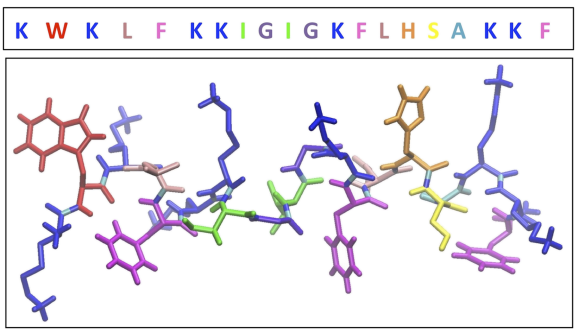

FIG. 1. Amino acid sequence and NMR structure (PDB-ID: 1D9J) of the cecropin A-magainin 2 hybrid peptide.

We also analyzed the effect of describing explicitly the hydrogen atoms on the rim of the SWCNT. For the hydrogenated SWCNT, the LJ were set to zero and partial charges on hydrogen and the corresponding bounded carbon atoms have been set to +0.1e and −0.1e, respectively, the same values used on the CH atoms of aromatic rings in the GROMOS54a7 force field. These values are in good agreement with those reported for SWCNT in the literature.[48] We have also analyzed the effect of a dipole inversion of the rim atoms by using a model in which the negatively charged fluorine atoms replace all rim hydrogens. In this case, we have opposite partial charges of the hydrogenated SWCNT model. The C–F distance was set to 0.134 nm and the LJ parameters were taken from the GROMOS54a7 library.[49]

For the peptide, the GROMOS54a7 force field[49] parameters were used for modeling the atomic interactions. The mixed LJ parameters for the interactions of the CNT/GNS carbon atoms with the peptide atoms were calculated using the GROMOS combination rules.[50] The Extended Simple Point Charge (SPC/E) model of water was used in all the simulations.[51]

The systems were set up by placing four CA-MA peptides and one GNS or SWCNT in the center of a cubic box with a length of 10 nm (see Figure S1 of the supplementary material). The remaining space was filled by stacking an equilibrated box of 216 water molecules and by removing any water molecule located within 0.25 nm from solute atoms. Chloride counter ions were added to keep the systems neutral. In Table I the compositions of the two systems are summarized. In the same table are also reported three simulations (1PC, 1PCF, and 1PCH) that have been performed starting from the configurations of one CNT of peptide 3 at time 254 ns from the 4PC simulation. These simulations have been solely used to study the effect of the rim functionalization on the entrance of the peptide in the CNT.

MD simulations protocol

The LINCS algorithm[52] had been applied in order to keep the covalent bonds constrained during the simulations. The

TABLE I. Composition and simulation length for all the systems studied.

System[a]	Number of peptides	Number of water	Number of Cl^-	Time/ns
4PG	4	32 211	32	350
4PC	4	32 242	32	350
1PC	1	32 644	8	100
1PCF	1	32 627	8	100
1PCH	1	32 627	8	100

[a]The numbers on the left side of the letter P indicate the number of peptides in the simulation, C and G stand for CNT and graphene, and F and H for the one-side fluorinated and hydrogenated rim of the nanotube.

integration time step was chosen to be 2 fs. A temperature of 300 K was maintained by Berendsen's thermostat[53] with a coupling time of 0.1 ps, and an isotropic pressure of 1.0 bar was maintained by Berendsen's barostat[53] with a coupling time of 0.5 ps. An isothermal compressibility of 4.5×10^{-5} bar^{-1} was used for all the simulations. The Particle mesh Ewald (PME) method[54] was applied for the long-range interactions with a real space cutoff of 1.0 nm and a Fourier mesh spacing of 0.12 nm. The LJ interactions were calculated using a cutoff of 1.4 nm.

All the MD simulations and analyses of the trajectories were performed using the GROMACS (version 4.5.5) software package.[55,56] The program VMD[57] was used to visualize the trajectories and create the graphical representation of the molecules. The secondary structure analysis of the peptides was performed using the DSSP method.[58]

The orientation of the side chain of the aromatic residues (Trp2, Phe5, Phe13, His15, Phe20) with respect to the graphene was determined using the following procedure. The GNS of each simulation frame was rotated and translated to fit its starting configuration, which was oriented perpendicular to the Z-axis of the reference system. The transformation matrix used to fit the graphene was also applied to the peptides. The normal vectors to the aromatic rings of the aforementioned amino acids were calculated using the three co-planar atoms (for Trp $C\delta_1, C\zeta_2, C\zeta_3$; for Phe, $C\delta_1, C\delta_2, C\varepsilon_2$; for His, $N\delta_1, C\varepsilon_1, N\varepsilon_2$). Finally, the normal vector was used to calculate the angle with the Z-axis, which ranges from 0° (or 180°) for parallel to the graphene plane to 90° for the perpendicular one. A similar approach was used to calculate the orientation with respect to the SWCNT surface. In this case, the nanotube from the simulations was fitted to the starting one oriented parallel to the Z-axis of the system. In this case, aromatic rings parallel to the SWCNT surface form an angle with the z-axis around 90° whereas those which are perpendicular form an angle around 0° (or 180°).

The radius of gyration was calculated from the trace of the gyration tensor. Diagonalization of the gyration tensor and ordering its principal moments (eigenvalues) such as $\lambda_1^2 > \lambda_2^2 > \lambda_3^2$ enable the calculation of the shape descriptors.[59] The asphericity b is given by

$$b = \lambda_1^2 - \frac{1}{2}\left(\lambda_2^2 + \lambda_3^2\right)$$

and the acylindricity $\boldsymbol{c}$ by

$$c = \left(\lambda_2^2 - \lambda_3^2\right).$$

The α-helix starting conformation is characterized by the following values: Rg = 1.1 nm, b = 0.93 nm^2, and c = 0.02 nm^2.

RESULTS

Interactions of CA-MA peptides with graphene nanosheet

The CA-MA peptide is to a large extent positively charged. Out of the twenty residues of the peptide, eight (seven lysines and one histidine) are positively charged without any negatively charged residues. Of the remaining residues, nine have a hydrophobic character (F, A, L, I, and W). Thus, the behavior of its adsorption at a hydrophobic surface cannot be easily

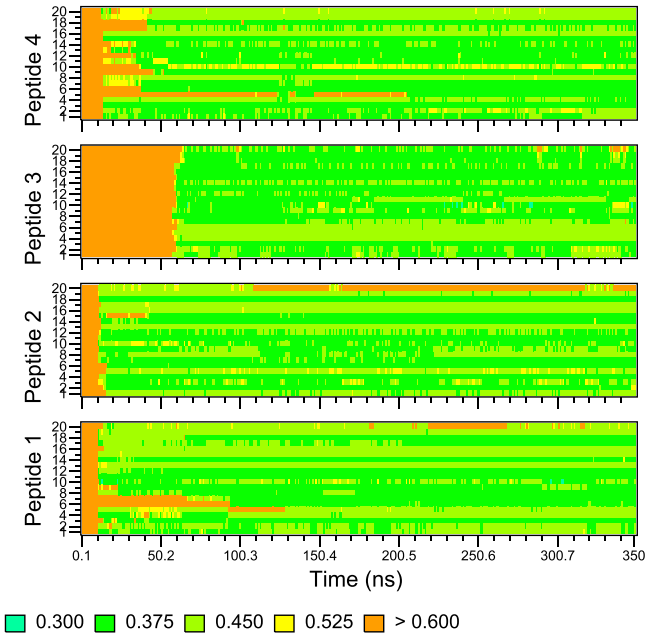

FIG. 2. Minimum distances between the Cα atoms of each peptide and the graphene carbon atoms.

predicted. We monitored the dynamics of its adsorption by calculating the distances between the peptide Cα atoms and the carbon atoms of the GNS. Figure 2 displays this minimum distance for each peptide as a function of time. Adsorption of peptides 1, 2, and 4 on one side of the graphene surface occurs during the first 10 ns of simulation. However, it takes 50 ns more for peptide 3 to bind to the GNS. This delay was because this peptide adsorbed at the farther face of the GNS and the extra time required for adsorption reflects the larger distance it had to diffuse. Nevertheless in all cases, after the initial adsorption, the peptides stayed in contact with the surface for the entire trajectory.

This confirms earlier reports that peptides and proteins are to some degree amphiphilic in the sense that they would be preferentially adsorbed at the hydrophilic–hydrophobic interface than reside in either of the bulk phases.[60–62] This property is predominantly determined by the bare backbone of the polypeptide chain and obviously can be altered by the identity of the side-chains.

In Figure 3(a) the top view of the peptides' configurations at the end of the simulation (350 ns) is reported. The peptides are adsorbed on both sides of the GNS with three of them on one side and the other on the opposite side. Therefore, the peptide surface density on the populated side is 0.11 peptide/nm^2 or 27 atoms/nm^2. It is likely that the migration of peptide 3 to the opposite face is because the closer face was too crowded to accept its adsorption. In this case, we can predict the saturation density of CA-MA hybrid peptide on graphene to be in the range 0.11-0.15 peptide/nm^2 or 27-35 atoms/nm^2. All peptides have a similar average Cα-GNS surface distance of 0.44 ± 0.03 nm indicating a nearly excluded volume contact with the graphene surface. In fact, the three peptides residing on the same face cover most of the GNS surface with a compact coating. The side chains of the aromatic amino acids (Trp2, Phe5, Phe13, His15, Phe20) tend to establish the closest contacts with the surface by orienting their aromatic rings

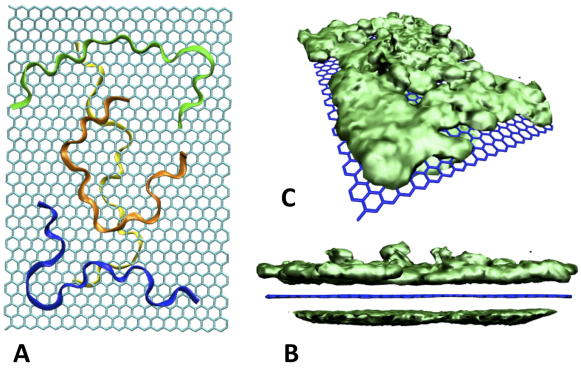

FIG. 3. The four CA-MA peptides on the GNS surface. (a) Top view of the configuration at 350 ns, the peptides are shown in ribbon representation. ((b) and (c)) Lateral view and top (perspective) view of the spatial density distribution of the peptides on the GNS surface. The average GNS conformation is reported as well.

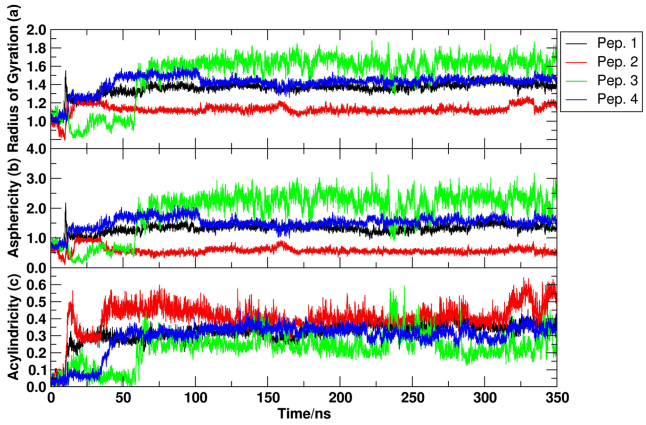

FIG. 4. From top to bottom panel: radius of gyration (in nm), asphericity (in nm^2), and acylindricity (in nm^2) for the 4 peptides (different colored curves) in the 4PG simulation.

parallel to the surface plane (see top panel of Figure S2 of the supplementary material). The distribution of their orientation with respect to the Z-axis of the reference system (oriented perpendicular to the graphene plane, see the section titled "Methods") is reported in the bottom panel of Figure S2 of the supplementary material. With the exception of the polar His15, the Trp2 shows distributions centered at ~90°.

Their packing interactions reduce the motions of the three peptides whereas the peptide on the other side being less restricted has larger fluctuations in the backbone structure.

In Figures 3(b) and 3(c), the spatial density distribution calculated in the last 100 ns of the simulation is reported. The upper surface with three peptides is highly corrugated. The side chains of charged and polar residues (Lys) protrude into the solvent creating a corrugated pattern on the crowded side of the graphene flake. In Figure S3 of the supplementary material, the averaged distance of the peptide atoms from the graphene average plane is reported. The highest peaks observed in peptides 2, 3, and 4 correspond to the side chain protruding into the solvents as observed in the density map (Figure 3).

They tower the surface extending for ~0.3 nm from the average position of the other peptide atoms. The accessibility of the side chain could be very important for anchoring the coated GNS surface to other molecules using, for example, polymeric linkers. The interaction of the peptides with the hydrophobic surface affects the stability of their initial α-helical configuration. Figure S4 of the supplementary material shows the change of the secondary structure of the four peptides during the simulation. A substantial decrease in the α-helical content occurs within the first 10 ns for all peptides except peptide 3. For the latter, additional 50 ns are required to lose the alpha-helix structure. This behavior correlates strongly with the adsorption behavior (see Figure 2). Thus, the adsorption of the peptide to the hydrophobic surface induces a complete loss of its alpha-helical structure (Figure 3(a)) and the formation of mainly random coil conformations. Concurrently to the loss of secondary structure due to the adsorption process, the peptide increases significantly its radius of gyration relative to the value in bulk water (for comparison, the modeled full extended β-stand configuration of the peptide is characterized by Rg = 2.1 nm, b = 4.2 nm^2, and c = 0.08 nm^2). This is shown in Figure 4 and Figure S5 of the supplementary material, together with the shape descriptors, the asphericity, and acylindricity.

At low density (thus, the case of peptide 3) the increase in the radius of gyration, as well as in the value of the asphericity, is larger than at high density (peptides 1, 2, and 4) a behavior that, as mentioned before, projects also on the local dynamics of the peptide. However at high density, although the radius of gyration is not very large, the acylindricity is larger than at low density. Nevertheless in all cases, the radius of gyration increases upon adsorption relative to the value in solution. The reason for the augmentation of the radius of gyration is because the random coil structure adopted upon adsorption is confined to the two-dimensional plane of the surface. The changes in the secondary structure and radius of gyration are also correlated with the distance from the surface (Figure S4 of the supplementary material).

Interaction of CA-MA with SWCNT

In Figure 5 the last configuration (after 350 ns) of each of the four CA-MA peptides interacting with the SWCNT is shown. Peptides 1, 3, and 4 are adsorbed on the nanotube's outer surface, whereas peptide 2, for almost its entire length, is inserted inside the CNT.

The process of adsorption of the four peptides was monitored by calculating the minimum distance between the Cα atoms of each peptide and the carbon atoms of the CNT along the simulation. In Figure 6, the plot of these distances is shown.

For peptides 3 and 4, a rapid adsorption (distances smaller than 0.5 nm) occurs after few nanoseconds. For peptides 1, 3, and 4 the adsorption occurs within 20 ns while for peptide 2 the contact with one of the nanotube entrances occurs only after ~250 ns. In Figure 7, the average distances calculated in the last 100 ns of the simulations between CNT surface atoms and those of the peptides are reported. The average distance for all atoms 0.6 nm from the CNT surface of peptides 1, 3, and 4 is 0.46 ± 0.06, and, for Cα atoms only, 0.44 ± 0.04 nm. The short distances indicate that peptides, once adsorbed on the SWCNT, remain in close contact for the rest of the simulation. As shown in Figure 5, peptides tend to maximize their contact

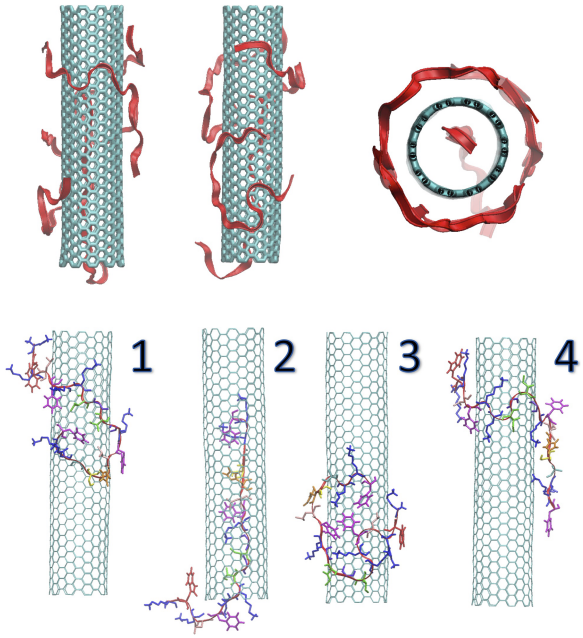

FIG. 5. Top: Snapshots of the last configuration from different angles (two side-views and one top view) of the 4PC simulation showing the arrangement of the four peptides (in ribbon) with the CNT (water molecules are omitted for clarity). Bottom: The same configuration but peptides are shown in a stick representation for a detailed view of the side chain orientations.

with the SWCNT surface by wrapping their backbone around it in a helical conformation.

The large peaks present in the graphs of the peptides 1 and 3 correspond to the side chains of the Lys residues that remain exposed to the solvent (see Figure 5, bottom panel). This behavior is consistent with the one observed for the peptides adsorbed on the GNS surface. The ionic layer produced by the charged side chains prevents peptide 2 to adsorb on the CNT outer surface forcing it (as for the peptide 3 in the GNS simulation) to search other favorable binding regions

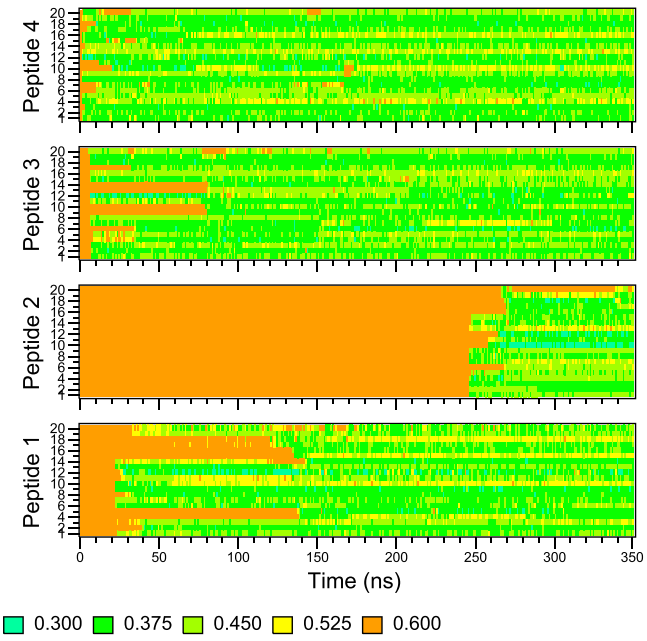

FIG. 6. Minimum distances between the Cα atoms in each peptide and the CNT surface.

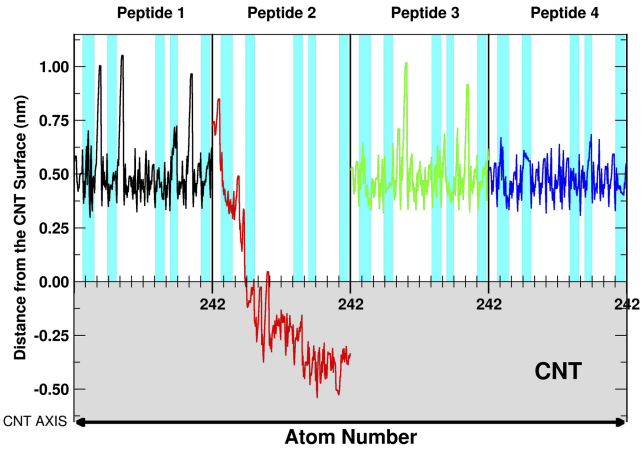

FIG. 7. The distances, averaged over the last 100 ns, of the 242 atoms of the peptides from the CNT principal axis that passes through its center. The cyan bars delimitate the 5 aromatic residues.

(namely the SWCNT internal surface). The peptide docking to the SWCNT rim required a time 2 orders of magnitude larger than the binding to the outer surface. The cyan bars indicate the position of aromatic residues (in the order Trp2, Phe5, Phe13, His15, Phe20). Also in the case of the SWCNT, the aromatic residues show a tendency to maximize their side chain contacts with the SWCNT (Figure 5, bottom panel) although the curvature of the cylindrical shaped SWCNT surface imposes an additional conformational constraint on the peptides. In Figure 8, the orientation angles of the aromatic size chain with respect to the SWCNT surface are reported. For all the peptides (also the peptide 2 inside the SWCNT), the distributions of the normal to the aromatic planes are centered in parallel (90°) or bended (75° or 110°) orientation with respect to the SWCNT axis showing a high propensity for these hydrophobic groups to maximize their contacts with the SWCNT surface.

We analyzed the changes in the peptide secondary structure (SS) along the trajectories in order to understand how the interaction with the CNT surface affects the initial peptide fold. Figure S6 of the supplementary material reports the content of the SSs for the four peptides. A decrease in the initial α-helical content occurs already at the beginning of simulation (within

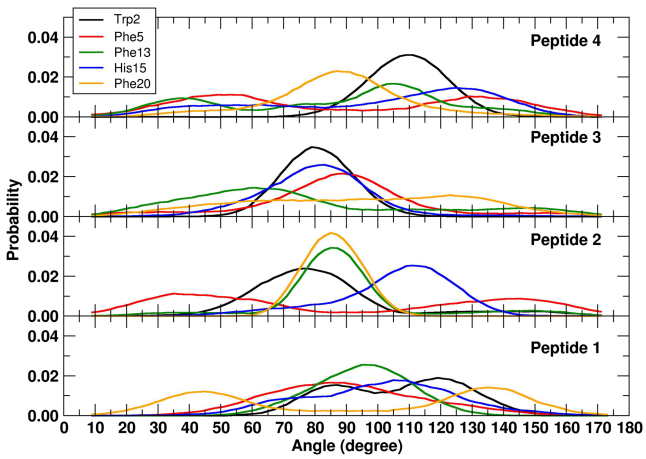

FIG. 8. Distribution of the angle between the normal to the plane of side chain aromatic residues and the Z-axis of the reference system, obtained from the last 100 ns of 4PC simulation.

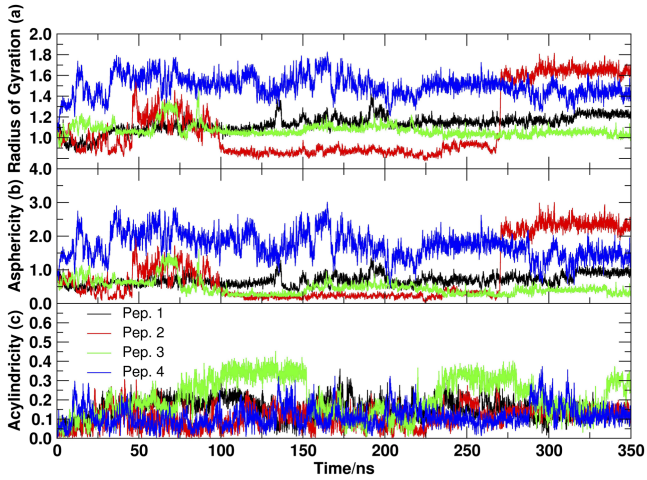

FIG. 9. From top to bottom panel: radius of gyration (in nm), asphericity (in nm^2), and acylindricity (in nm^2) for the 4 peptides (different colored curves) in the 4PC simulation.

10–50 ns) for all the peptides. After 150 ns, a complete loss of the α-helical content is observed. For the rest of the simulation, the SSs are characterized by the presence of β-strands and β-bridges distributed at different regions of the peptide. However, as for the simulation with GNS, at the end of the simulation the peptides adopt mostly random coil conformations. Thus, the behavior of the four peptides is quite similar except for the case of peptide 2 where the insertion of the peptide into the CNT (at ~240 ns) is correlated with an extended coil conformation for the intruding segment. It is worth noting that the rate of the loss of secondary structure is slightly slower than for the case in which the peptides interact with the planar GNS surface.

In Figure 9, the radii of gyration and the two shape descriptors of the four peptides in the presence of the CNT are reported. Similar to the behavior of the peptides when they are adsorbed on GNS, the value of their radius of gyration is much larger than in bulk. Again this is a result of the loss of the globular folded conformation of the peptides and the adoption of a more extended structure that maximizes their binding to the CNT. By wrapping around the structure of the carbon tube, the values of the acylindricity parameter, c, are significantly smaller than those obtained when the peptides are adsorbed on graphene. Nevertheless, the values of the asphericity parameter are similar (see Figure 4 for comparison).

Diffusion of the peptide inside the CNT

In Figure S7 of the supplementary material, different stages of the insertion process of peptide 2 into the CNT are shown. For clarity other peptides and water molecules are omitted. The process is initiated by the penetration of the neutral C-terminal of the peptide at ~264 ns and proceeds for ~50 ns (until 315 ns). After this time, the N-terminal of the peptide remains anchored to the outer surface of the CNT impeding further diffusion into the CNT for the rest of the simulation. Thus, it seems that the bottleneck for the insertion process is the search for the entrance to the nanotube interior by the C-terminal. Note that after the initial insertion, the peptide proceeds to diffuse rapidly inside the nanotube penetrating 3/4 (~4.5 nm) of the CNT length (6 nm) with an average speed of ~0.09 nm/ns or 0.3 residues/ns.

Effect of the charges on the CNT rim

The spontaneous insertion of peptide 2 occurred with the united-atom model for the carbon atoms at the rim of the SWCNT having a zero partial charge. We now examine whether this process occurs also in the presence of explicitly charged atoms on the rim of the SWCNT. QM calculations on SWCNT models (see the section titled "Methods") have shown the presence of a partial charge distribution between the carbon and the bounded hydrogen atoms that determine the formation of small dipoles around the rim of the SWCNT. Therefore, we have analysed the effect of these dipoles on the peptide insertion mechanism by adding either hydrogen or fluorine to atoms of carbon on one end of the SWCNT (see the section titled "Methods"). We have kept the carbon atoms at the other end of the SWCNT as united carbon atoms. Hence, we have performed two new simulations starting with the hydrogenated and fluorinated SWCNTs (Table I, 1PCH and 1PCF simulations, respectively) and only peptide 2 in the same starting configuration as the one obtained at 264 ns of the 4PC simulation (see Figure S6 of the supplementary material). An additional simulation with the united-atom SWCNT model was run as control.

In Figures 10(a)–10(c) five snapshots from each simulation describing the diffusion process of the peptide inside the united-atom (Figure 10(a)), fluorinated (Figure 10(b)), and hydrogenated SWCNT (Figure 10(c)) are shown. The plots at the bottom of each figure and in Figure S8 of the supplementary material represent the minimum distance between the C-α atom of residue F20 and the carbon atoms in the top rim of the SWCNT along each simulation. The figure shows that the insertion into the SWCNT interior takes place in the case of the 1PC and 1PCF simulations but not in the 1PCH one. In both the cases, the insertion takes place from the C-terminal region of the peptide. In this region, two positively charged residues (-K18-K19-) are present. As mentioned above, there is a free energy barrier for the C-terminal to find and enter the entrance rim. Therefore, the negatively charged fluorine atoms are likely to reduce this barrier by favorably interacting with the positively charged C-terminal regions of the peptide. A relatively low free energy barrier also exists at the neutral rim of the united-atoms SWCNT due to the terminal F20. In both cases, the peptide docks with the nanotube entrance in a short time (0.5 ns for the united-atoms and 0.8 ns for the fluorinated one, top and middle graph of Figure S8 of the supplementary material). The insertion of the peptide 3 nm inside the nanotube is two times faster for the united atoms than the fluorinated one (which can be explained by the attraction of the negatively charged rim to the positively charged residues). However, peptide in the fluorinated one completes the insertion in a time 2.3 times faster (~29 ns) than the united atom (~66 ns). As shown in Figure S8 of the supplementary material, in both cases, the insertion process occurs in three fast steps separated by intervals of no insertion (regions in cyan color in Figure S8 of the supplementary material, top and middle panels). For the 1PC simulation, the approximate speeds in the three insertion events are 0.2 nm/ns (1.5 residues/ns),

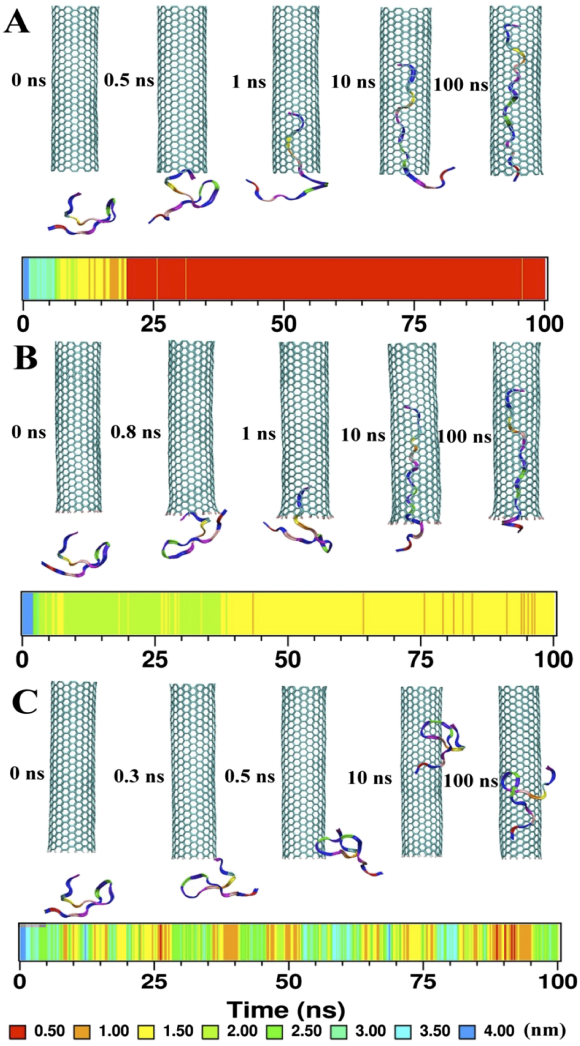

FIG. 10. Snapshots from the simulations showing the peptide diffusion into the SWCNT interior with (a) united carbon atoms and (b) fluorinated rim at the edge closest to the peptide. In (c) the SWCNT rim was hydrogenated; however, the peptide did not enter into the nanotube. The color band plots below each set of snapshots show the distance between the C-terminal F20 (Cα atom) of the peptide and the rim of the nanotube along the simulation. The color-coding of distances is indicated in the legend at the bottom.

1.3 nm/ns (4.3 residues/ns), and 0.23 nm/ns (0.77 residues/ns), respectively. For the 1PCF simulation, the speeds are 0.12 nm/ns (0.4 residues/ns), 0.42 nm/ns (1.4 residue/ns), and 0.91 nm/ns (3 residues/ns), respectively. In both cases, there is an insertion event that occurs at the highest speed of 3-4 amino acids/ns. At the end of the simulation (100 ns), the peptide is fully inserted inside the uncharged nanotube.

In Figure S10 of the supplementary material, the distances between the Cα of the Lys1 and Phe20 are reported for the three simulations. The peptide in the united atoms SWCNT has a more extended conformation than in the fluorinated SWCNT in which the N-terminal part of the peptide remains outside of the nanotube (see the last snapshot in Figure 10(b)). The N-terminal of the peptide contains the two positively charged amino acids Lys1 and Lys3 that electrostatically interact with the negatively charged fluorine atoms on the rim.

In contrast to the united-atom and the fluorinated SWCNTs, the peptide does not insert into the nanotube with the explicit hydrogen atoms on the rim (see Figure 10(c) and the bottom plot of Figure S8 of the supplementary material) but it only adsorbs on its surface. A possible explanation of this behavior is related to the electrostatic repulsion between the hydrogen atoms on the SWCNT rims and the positively charged residues present on the C-terminal part of the peptide. The repulsive interactions raise the insertion free energy barrier preventing the peptide from entering the nanotube and diverting it on the SWCNT surface. The distance between the C-terminal and the SWCNT rim atoms exhibits periodic oscillations (see bottom panel of Figure S8 of the supplementary material). The peptide end-to-end distance in the last 80 ns of the simulation does not show a large variation from its average value of ~2.5 nm (Figure S9 of the supplementary material), indicating that the peptide remains adsorbed on the outer surface of the SWCNT sliding back and forth on its surface in the conformation shown in the bottom panel of Figure 10. An oscillation period of 12.5 ns was obtained from the discrete Fourier transform of the end-to-end distance (largest peak in the inset of Figure S9 of the supplementary material).

DISCUSSION AND CONCLUSIONS

MD simulations were performed to study the mechanism of interaction of hybrid antimicrobial peptide CA-MA with a CNT (10, 10) and a graphene nanosheet with the same surface area. The MD results show that in both cases the CA-MA peptides adsorb to these carbon-based surfaces. As the peptides approach the surface, they completely lose their secondary structure. We have recently shown that the same peptide in pure water tends to retain a stable secondary.[38] Note that in other cases, the loss of the alpha-helical content of the peptide upon adsorption onto a hydrophobic surface can be accompanied by the formation of fibril aggregates as reported for the amyloid beta (Aβ) (1-42).[63,64]

The peptide residues that were found to bind closest to the graphene surface are the aromatic amino acids such as tryptophanes, phenylalanines, and histidines, likely due to favorable direct dispersion as well as solvent-induced interactions with the flat surface. This result is in agreement with those obtained by Wang *et al.*[21] In their scanning electron microscopy (SEM) study, it was found that peptides displaying high affinity with the nanotube surface are rich in histidine and tryptophan residues.[21] In addition, MD simulations by Tomásio and Walsh[39] demonstrated that the ability of tryptophan rich peptides to adsorb on carbon nano-surfaces is reduced when the large aromatic residue tryptophan is substituted by smaller aromatic residues such as tyrosine or phenylalanine. Furthermore, our simulations indicate that the CA-MA peptides expose most of the functionalizable Lys side-chains towards the aqueous solvents.

The protrusion is more evident in the SWCNT than in the GNS. This is likely a result of the higher curvature of the CNT surface which renders the binding of the peptide to the surface weaker and thereby facilitating the intrusion of the Lys residues into the aqueous solution.

With regards to the interaction with CNT, we find that the CA-MA peptide prefers first to adsorb at the outer surface of the CNT and only when this surface is occupied does it insert into the tube interior. As for the GNS, aromatic amino acids tend to gain dispersive interaction energy by orienting

their aromatic ring parallel to the surface. This effect was observed in previous simulations of peptides[39] or polymers[65] with carbon surfaces.

Similar to the simulation with graphene and also with the SWCNT, the adsorption induces unfolding. This behavior is likely to depend on the radius of the CNT and the properties of the peptides. For example, simulations by Trzaskowski *et al.*[40] reported no change in secondary structure contents of α-helix and β-hairpin model peptides when interacting with the outer and inner walls of CNTs. In this case, the two SWCNTs considered were with chiral indices of (22, 0) and (30, 0), respectively. Nevertheless when the peptide was covalently bonded to the nanotube via a linker, significant changes in the secondary structure were observed. Sansom and co-workers[42] also reported a change in the alpha-helical content of a peptide when it adsorbs on the CNT at low peptide concentration. Zuo *et al.*,[44] in a study on the adsorption of protein villin headpiece onto graphene, also reported secondary structure changes.

From the results obtained from our simulations, we cannot conclude that the binding of the peptide to the GNS is stronger than that to the CNT. However, does the shape of the surface make a difference to the extent of the unfolding? A study by Balamurugan *et al.*[43] suggests that alpha-helical peptides lose their structure more when adsorbed to GNS than to CNT because the former has a smaller curvature. These results imply that the degree of unfolding increases for stronger peptide-surface interaction energy. This is very reasonable because favorable interactions of the peptide with the surface can compensate for the loss of intra-peptide interactions in the folded state.

The unfolded peptide chains maximize their contacts with the SWCNT surface by wrapping around it. This adsorption mechanism was observed in a linear block copolymer with hydrophobic units;[66] the presence of aromatic residues plays an important role in SWCNT polymer binding.[39,67] In general, the non-covalent wrapping of carbon nanotubes by polymers plays an important role as a functional dispersant and has been recently extensively reviewed.[68] For peptides, the importance of aromatic amino acids in adsorption to SWCNT was experimentally investigated using peptides of different compositions.[69] Peptides having higher content of Phe amino acids have shown a larger tendency to disperse SWCNT in solution.[69]

In our simulation, we have also observed a spontaneous insertion of one of the 4 peptides into the interior of the SWCNT. The insertion occurs only when the outer surface had already been occupied by other peptides. The spontaneity of the process is possibly due to the strong peptide-surface interaction energy because inside the CNT the peptide loses a significant amount of its conformational entropy. The insertion occurs in a time scale of 30-60 ns at the highest speed of 3-4 amino acids/ns. Furthermore, we find that by modifying the electrostatic interactions between the peptide and the nanotube rims, the encapsulation of the peptide into the nanotube can be controlled.

The insertion of a 17 amino acid long α-helix peptide in armchair (14, 14) and a zigzag (24, 0) SWCNT of diameters 1.88 nm and 1.90 nm, respectively, was recently reported.[70] Due to the larger diameter of the SWCNT, the complete encapsulation of the peptide in the armchair SWCNT is ~3 times faster than in our case; for the zigzag SWCNT they observed a trapping of the peptide after 20 ns that could be due to the different structure of the SWCNT rim. Similar to our results, the peptide lost its secondary structure adopting a random conformation.

The conformation loss is also in agreement with other studies of α-helical peptides (in particular a-helix forming peptides) confined inside SWCNT with diameters ranging from ~0.15 to ~0.35 nm.[71,72] In all these studies, the peptides were confined in the nanotube and the spontaneous encapsulation was not directly observed. Although other simulations did observe spontaneous encapsulation of a large peptide into SWCNT, to the best of our knowledge, the nanotube in our study has the smallest diameter.

The results of this study evidenced the tendency of the selected AMP peptide to non-covalently absorb on and encapsulate into a small ultra-short SWCNT. These results could be of interest for potential applications in nanotechnology, biotechnology, and nanomedicine.[73] For example, the strong tendency of the peptide to coat the surface of the nanomaterial is already exploited for enhancing the solubility of both GNSs and SWCNT preventing their aggregation in water.[74–77] This strong interaction tendency could be exploited to create a peptide based non-covalent anchoring system. In this way, an active molecule could be attached to the anchoring peptide by appropriate spacing at the peptide termini or at the protruding amino acids (Lys and Arg). Hence, by providing an appropriate release mechanism of the linker molecule triggered, for example, by temperature, pH, or chemical condition, it could be possible to build a smart drug delivery system or an active surface. In the case of drug delivery systems, there is a demonstrated tendency of both SWCNT and GNS to cumulate inside cells increasing the peptide concentration and thus enhancing its bactericide activity.[78–80]

SUPPLEMENTARY MATERIAL

See supplementary material for structural details of the final structure from the simulations, plot of secondary structures along the simulations, plots of distances from the graphene and CNT surfaces, plots of radius of gyration, asphericity and acylindricity for peptides in the pure water simulation, plots of distance of peptides from the CNT rims. This material is available free of charge via the Internet at http://pubs.acs.org.

ACKNOWLEDGMENTS

We would like to acknowledge the computational resources of Computational Laboratory for Analysis, Modelling, and Visualizations (CLAMV) at Jacobs University of Bremen, Germany. E.S. additionally thanks the international Ph.D. program between the University of Salerno and Jacobs University of Bremen for the financial support.

[1] R. H. Baughman, A. A. Zakhidov, and W. A. de Heer, Science **297**, 787–792 (2002).
[2] R. H. Baughman, C. Cui, A. A. Zakhidov, Z. Iqbal, J. N. Barisci, G. M. Spinks, G. G. Wallace, A. Mazzoldi, D. De Rossi, and A. G. Rinzler, Science **284**, 1340–1344 (1999).

[3]X. Liu, L. Shi, W. Niu, H. Li, and G. Xu, Biosens. Bioelectron. **23**, 1887–1890 (2008).
[4]B. L. Allen, P. D. Kichambare, and A. Star, Adv. Mater. **19**, 1439–1451 (2007).
[5]S. Dhar, Z. Liu, J. Thomale, H. Dai, and S. J. Lippard, J. Am. Chem. Soc. **130**, 11467–11476 (2008).
[6]H. G. Boman, "Peptide antibiotics and their role in innate immunity," Annu. Rev. Immunol. **13**, 61–92 (1995).
[7]K. A. Brogden, Nat. Rev. Microbiol. **3**, 238–250 (2005).
[8]R. E. W. Hancock and A. Rozek, FEMS Microbiol. Lett. **206**, 143–149 (2002).
[9]W. L. Maloy and U. P. Kari, Biopolymers **37**, 105–122 (1995).
[10]M. Zasloff, Curr. Opin. Immunol. **4**, 3–7 (1992).
[11]V. L. Colvin, Nat. Biotechnol. **21**, 1166–1170 (2003).
[12]D. Cui, F. Tian, C. S. Ozkan, M. Wang, and H. Gao, Toxicol. Lett. **155**, 73–85 (2005).
[13]C.-W. Lam, J. T. James, R. McCluskey, and R. L. Hunter, Toxicol. Sci. **77**, 126–134 (2004).
[14]A. Magrez, S. Kasas, V. Salicio, N. Pasquier, J. W. Seo, M. Celio, S. Catsicas, B. Schwaller, and L. Forró, Nano Lett. **6**, 1121–1125 (2006).
[15]N. A. Monteiro-Riviere, R. J. Nemanich, A. O. Inman, Y. Y. Wang, and J. E. Riviere, Toxicol. Lett. **155**, 377–384 (2005).
[16]W. Huang, S. Fernando, L. F. Allard, and Y.-P. Sun, Nano Lett. **3**, 565–568 (2003).
[17]J. E. Riggs, Z. Guo, D. L. Carroll, and Y.-P. Sun, J. Am. Chem. Soc. **122**, 5879–5880 (2000).
[18]M. Granite, A. Radulescu, W. Pyckhout-Hintzen, and Y. Cohen, Langmuir **27**, 751–759 (2011).
[19]J. U. Lee, J. Huh, K. H. Kim, C. Park, and W. H. Jo, Carbon **45**, 1051–1057 (2007).
[20]K. Min, J. Kim, K. Park, and Y. J. Yoo, J. Mol. Catal. B: Enzym. **83**, 87–93 (2012).
[21]S. Wang, E. S. Humphreys, S.-Y. Chung, D. F. Delduco, S. R. Lustig, H. Wang, K. N. Parker, N. W. Rizzo, S. Subramoney, and Y.-M. Chiang, Nat. Mater. **2**, 196–200 (2003).
[22]R. R. Johnson, A. C. Johnson, and M. L. Klein, Nano Lett. **8**, 69–75 (2008).
[23]J. Y. Lee, A. Boman, C. X. Sun, M. Andersson, H. Jornvall, V. Mutt, and H. G. Boman, Proc. Natl. Acad. Sci. U. S. A. **86**, 9159–9162 (1989).
[24]S. Y. Shin, J. H. Kang, M. K. Lee, S. Y. Kim, Y. M. Kim, and K. S. Hahm, Biochem. Mol. Biol. Int. **44**, 1119–1126 (1998).
[25]H. Steiner, D. Hultmark, A. Engstrom, H. Bennich, and H. G. Boman, Nature **292**, 246–248 (1981).
[26]Y. Sang and F. Blecha, Anim. Health Res. Rev. **9**, 227–235 (2008).
[27]R. E. W. Hancock, Lancet **349**, 418–422 (1997).
[28]D. Oh, S. Y. Shin, S. Lee, J. H. Kang, S. D. Kim, P. D. Ryu, K.-S. Hahm, and Y. Kim, Biochemistry **39**, 11855–11864 (2000).
[29]B. Bechinger, Biochim. Biophys. Acta, Biomembr. **1462**, 157–183 (1999).
[30]H. G. Boman, Cell **65**, 205–207 (1991).
[31]D. Hultmark, H. Steiner, T. Rasmuson, and H. G. Boman, Eur. J. Biochem. **106**, 7–16 (1980).
[32]H. G. Boman, I. Faye, P. Vonhofsten, K. Kockum, J. Y. Lee, K. G. Xanthopoulos, H. Bennich, A. Engstrom, R. B. Merrifield, and D. Andreu, Dev. Comp. Immunol. **9**, 551–558 (1985).
[33]R. I. Lehrer and T. Ganz, Curr. Opin. Immunol. **11**, 23–27 (1999).
[34]C. L. Bevins and M. Zasloff, Annu. Rev. Biochem. **59**, 395–414 (1990).
[35]M. Zasloff, Proc. Natl. Acad. Sci. U. S. A. **84**, 5449–5453 (1987).
[36]E. Soravia, G. Martini, and M. Zasloff, FEBS Lett. **228**, 337–340 (1988).
[37]D. Oh, Y. Kim, S. Y. Shin, J. H. Kang, K. S. Hahm, and K. L. Kim, J. Pept. Res. **53**, 578–589 (1999).
[38]E. Sarukhanyan, G. Milano, and D. Roccatano, Biopolymers **103**, 1–14 (2015).
[39]S. M. Tomásio and T. R. Walsh, J. Phys. Chem. C **113**, 8778–8785 (2009).
[40]B. Trzaskowski, A. F. Jalbout, and L. Adamowicz, Chem. Phys. Lett. **430**, 97–100 (2006).
[41]C.-c. Chiu, G. R. Dieckmann, and S. O. Nielsen, J. Phys. Chem. B **112**, 16326–16333 (2008).
[42]E. J. Wallace, R. S. D'Rozario, B. M. Sanchez, and M. S. Sansom, Nanoscale **2**, 967–975 (2010).
[43]K. Balamurugan, E. A. Singam, and V. Subramanian, J. Phys. Chem. C **115**, 8886–8892 (2011).
[44]G. Zuo, X. Zhou, Q. Huang, H. Fang, and R. Zhou, J. Phys. Chem. C **115**, 23323–23328 (2011).
[45]G. Gianese, V. Rosato, F. Cleri, M. Celino, and P. Morales, J. Phys. Chem. B **113**, 12105–12112 (2009).
[46]J. H. Walther, R. Jaffe, T. Halicioglu, and P. Koumoutsakos, J. Phys. Chem. B **105**, 9980–9987 (2001).
[47]T. Werder, J. H. Walther, R. Jaffe, T. Halicioglu, and P. Koumoutsakos, J. Phys. Chem. B **107**, 1345–1352 (2003).
[48]D. Lu, Y. Li, U. Ravaioli, and K. Schulten, J. Phys. Chem. B **109**, 11461–11467 (2005).
[49]N. Schmid, A. P. Eichenberger, A. Choutko, S. Riniker, M. Winger, A. E. Mark, and W. F. van Gunsteren, Eur. Biophys. J. **40**, 843–856 (2011).
[50]W. F. van Gunsteren, S. R. Billeter, A. A. Eising, P. H. Hünenberger, P. Krüger, A. E. Mark, W. R. P. Scott, and I. G. Tironi, *Biomolecular Simulation: The GROMOS96 Manual and User Guide* (Hochschuleverlag AG an der ETH Zürich, 1996).
[51]H. J. C. Berendsen, J. R. Grigera, and T. P. Straatsma, J. Phys. Chem. **91**, 6269–6271 (1987).
[52]B. Hess, H. Bekker, H. J. C. Berendsen, and J. G. E. M. Fraaije, J. Comput. Chem. **18**, 1463–1472 (1997).
[53]H. J. C. Berendsen, J. P. M. Postma, W. F. Vangunsteren, A. Dinola, and J. R. Haak, J. Chem. Phys. **81**, 3684–3690 (1984).
[54]T. Darden, D. York, and L. Pedersen, J. Chem. Phys. **98**, 10089–10092 (1993).
[55]B. Hess, C. Kutzner, D. van der Spoel, and E. Lindahl, J. Chem. Theory Comput. **4**, 435–447 (2008).
[56]H. J. C. Berendsen, D. Vanderspoel, and R. Vandrunen, Comput. Phys. Commun. **91**, 43–56 (1995).
[57]W. Humphrey, A. Dalke, and K. Schulten, J. Mol. Graphics **14**, 33–38 (1996).
[58]W. Kabsch and C. Sander, Biopolymers **22**, 2577–2637 (1983).
[59]D. N. Theodorou and U. W. Suter, Macromolecules **18**, 1206–1214 (1985).
[60]M. Karlsson, J. Ekeroth, H. Elwing, and U. Carlsson, J. Biol. Chem. **280**, 25558–25564 (2005).
[61]J.-H. Kim and J.-Y. Yoon, *Protein Adsorption on Polymer Particles* (Marcel Dekker, Inc., New York, 2002), Vol. 1, p. 4373.
[62]G. Raffaini and F. Ganazzoli, Langmuir **26**, 5679–5689 (2010).
[63]B. Moores, E. Drolle, S. J. Attwood, J. Simons, and Z. Leonenko, PLoS One **6**, e25954 (2011).
[64]X. Yu, Q. Wang, Y. Lin, J. Zhao, C. Zhao, and J. Zheng, Langmuir **28**, 6595–6605 (2012).
[65]M. Yang, V. Koutsos, and M. Zaiser, J. Phys. Chem. B **109**, 10009–10014 (2005).
[66]E. Sarukhanyan, G. Milano, and D. Roccatano, J. Phys. Chem. C **118**, 18069–18078 (2014).
[67]S. S. Tallury and M. A. Pasquinelli, J. Phys. Chem. B **114**, 9349–9355 (2010).
[68]T. Fujigaya and N. Nakashima, Sci. Technol. Adv. Mater. **16**, 024802 (2015).
[69]V. Zorbas, A. L. Smith, H. Xie, A. Ortiz-Acevedo, A. B. Dalton, G. R. Dieckmann, R. K. Draper, R. H. Baughman, and I. H. Musselman, J. Am. Chem. Soc. **127**, 12323–12328 (2005).
[70]Z. S. Zhang, Y. Kang, L. J. Liang, Y. C. Liu, T. Wu, and Q. Wang, Biomaterials **35**, 1771–1778 (2014).
[71]E. J. Sorin and V. S. Pande, J. Am. Chem. Soc. **128**, 6316–6317 (2006).
[72]E. P. O'Brien, G. Stan, D. Thirumalai, and B. R. Brooks, Nano Lett. **8**, 3702–3708 (2008).
[73]C. J. Serpell, K. Kostarelos, and B. G. Davis, ACS Cent. Sci. **2**, 190–200 (2016).
[74]E. L. Bakota, L. Aulisa, D. A. Tsyboulski, R. B. Weisman, and J. D. Hartgerink, Biomacromolecules **10**, 2201–2206 (2009).
[75]G. R. Dieckmann, A. B. Dalton, P. A. Johnson, J. Razal, J. Chen, G. M. Giordano, E. Munoz, I. H. Musselman, R. H. Baughman, and R. K. Draper, J. Am. Chem. Soc. **125**, 1770–1777 (2003).
[76]A. Ortiz-Acevedo, H. Xie, V. Zorbas, W. M. Sampson, A. B. Dalton, R. H. Baughman, R. K. Draper, I. H. Musselman, and G. R. Dieckmann, J. Am. Chem. Soc. **127**, 9512–9517 (2005).
[77]J. Montenegro, C. Vazquez-Vazquez, A. Kalinin, K. E. Geckeler, and J. R. Granja, J. Am. Chem. Soc. **136**, 2484–2491 (2014).
[78]P. D. Boyer, S. Ganesh, Z. Qin, B. D. Holt, M. J. Buehler, M. F. Islam, and K. N. Dahl, ACS Appl. Mater. Interfaces **8**, 3524–3534 (2016).
[79]X. Zou, L. Zhang, Z. Wang, and Y. Luo, J. Am. Chem. Soc. **138**, 2064–2077 (2016).
[80]M. Adeli, R. Soleyman, Z. Beiranvand, and F. Madani, Chem. Soc. Rev. **42**, 5231–5256 (2013).

Supplementary Materials:

Adsorption Mechanism of an Antimicrobial Peptide on Carbonaceous Surfaces: A Molecular Dynamics Study

Danilo Roccatano[1,1)], Edita Sarukhanyan[2,2)], Ronen Zangi[3,4]

[1] *School of Mathematics and Physics, University of Lincoln, Brayford Pool, Lincoln, LN6 7TS, United Kingdom.*

[2] *School of Engineering and Science, Jacobs University Bremen, Campus Ring 1, 28759 Bremen, Germany.*

[3] *Polymat & Department of Organic Chemistry I, University of the Basque Country UPV/EHU, Avenida de Tolosa 72, 20018, San Sebastian, Spain.*

[4] *IKERBASQUE, Basque Foundation for Science, Maria Diaz de Haro 3, 48013 Bilbao, Spain.*

I Contents

[1] Author to whom correspondence should be addressed. Electronic mail: droccatano@lincoln.ac.uk

[2] Current Address: Department of Bioinformatics, Biozentrum, Universität Würzburg,Am Hubland, D-97074 Wuerzburg, Germany.

Figure S8. Graphs of the variations in time of the distance between the F20 (C-α atom) of the peptide and the carbon atoms on the rim of the SWCNT. Top: SWCNT with united atoms on the rim (1PC simulation). Middle: SWCNT with one-side fluorinated nanotube (1PCF simulation). Bottom: SWCNT with one-side protonated nanotube (1PCH simulation).

Figure S9. Time series of the distance between the Cα atoms of Lys1 and Phe20 of the peptide during the 1PC, 1PCF, 1PCH simulations.

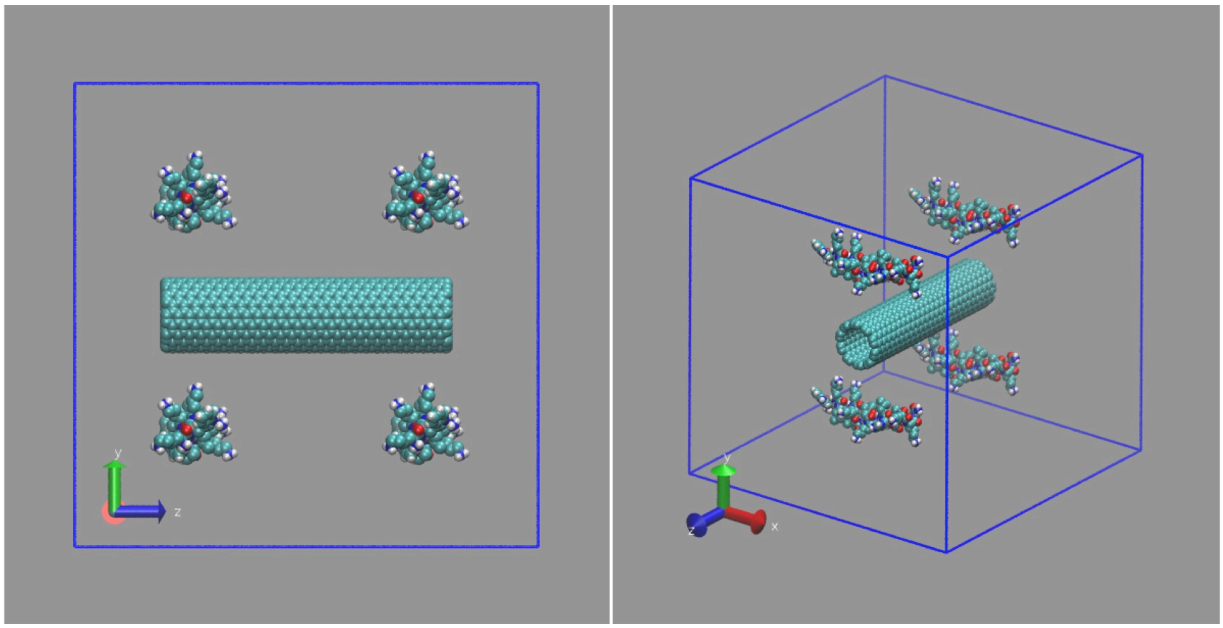

Figure S1. Starting configuration of the 4 peptides around the CNT in the simulation 4PC.

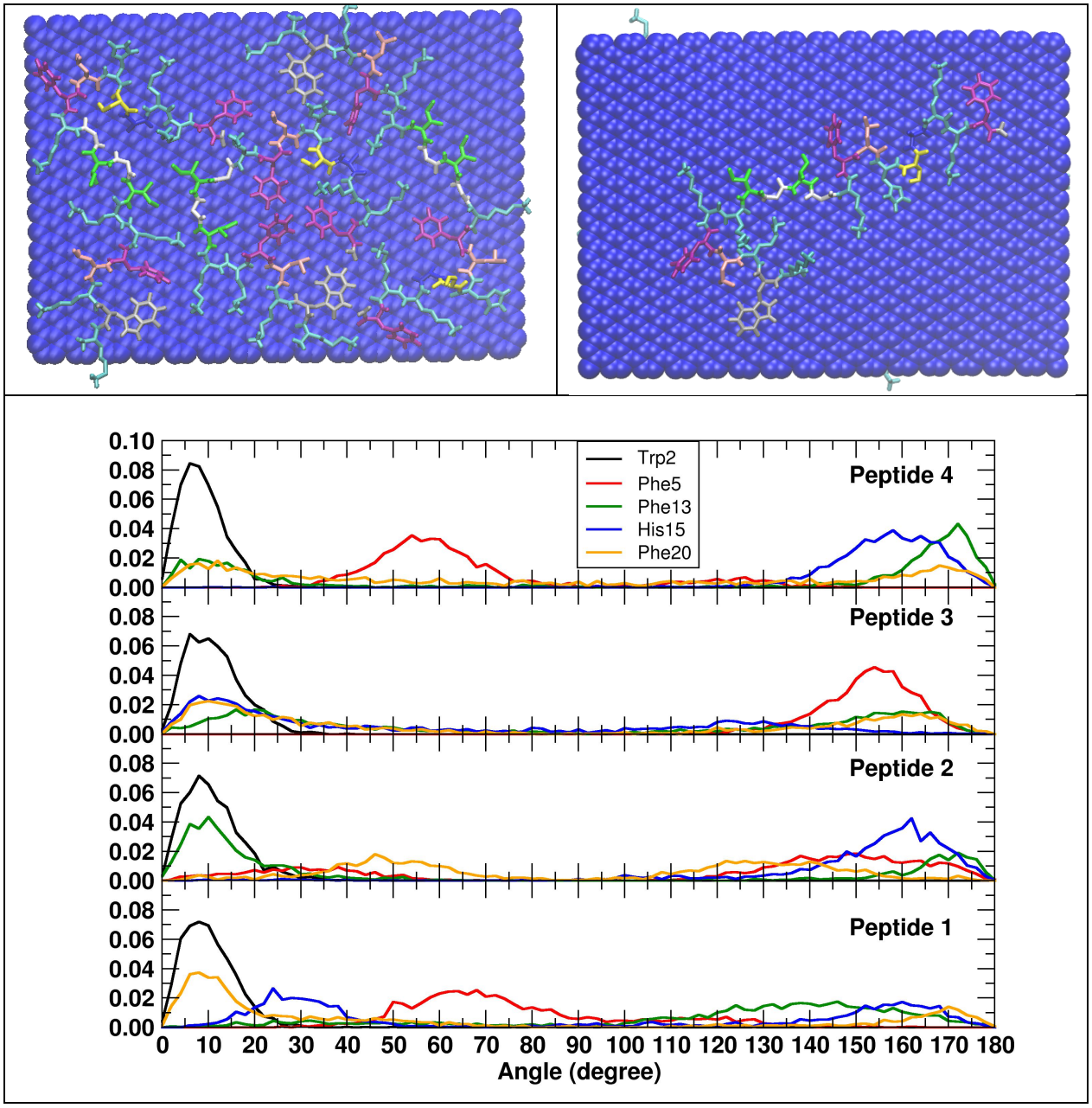

Figure S2. Top. Last frame (350 ns) of the simulation 4PG. The peptides are shown in stick representation on both the sides of the graphene. Bottom. Distribution of the angle between the normal to the plane of side chains of aromatics residues and the Z-axis of the reference system, obtained from the last 100 ns of the 4PG simulation.

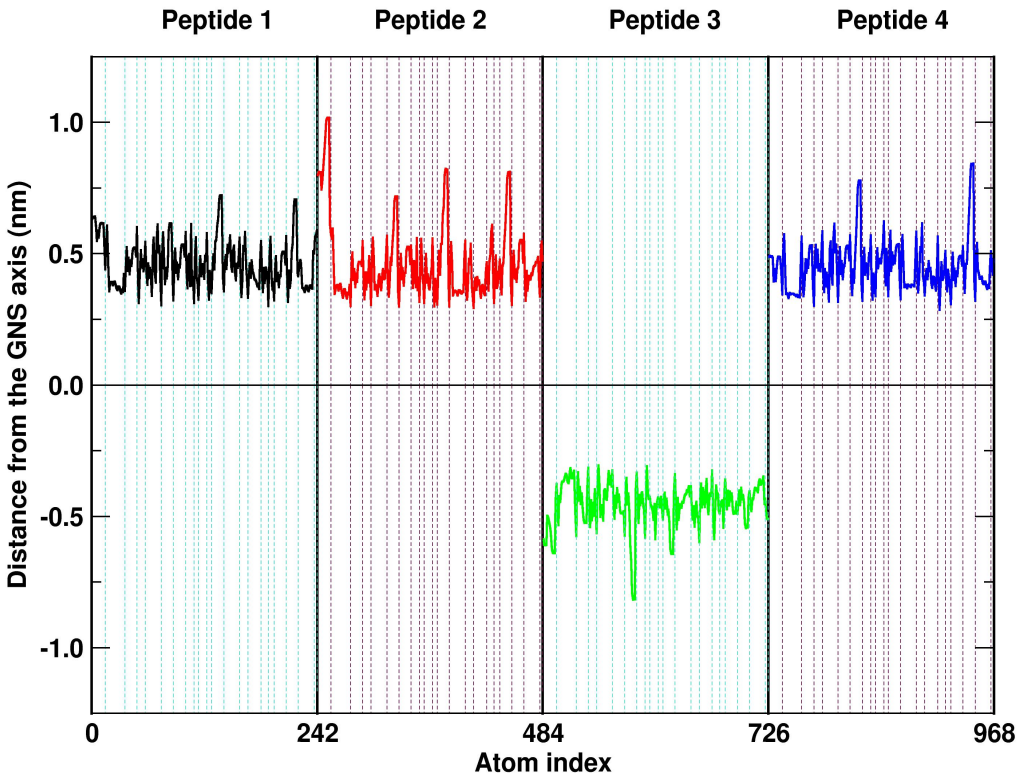

Figure S3. Distance of the single atoms of the 4 peptides from the GNS surface calculated using the last 100 ns of the simulation. The sign of the distance indicate the position of the peptides with respected the GNS plane. The dashed lines delimitate the single amino acids.

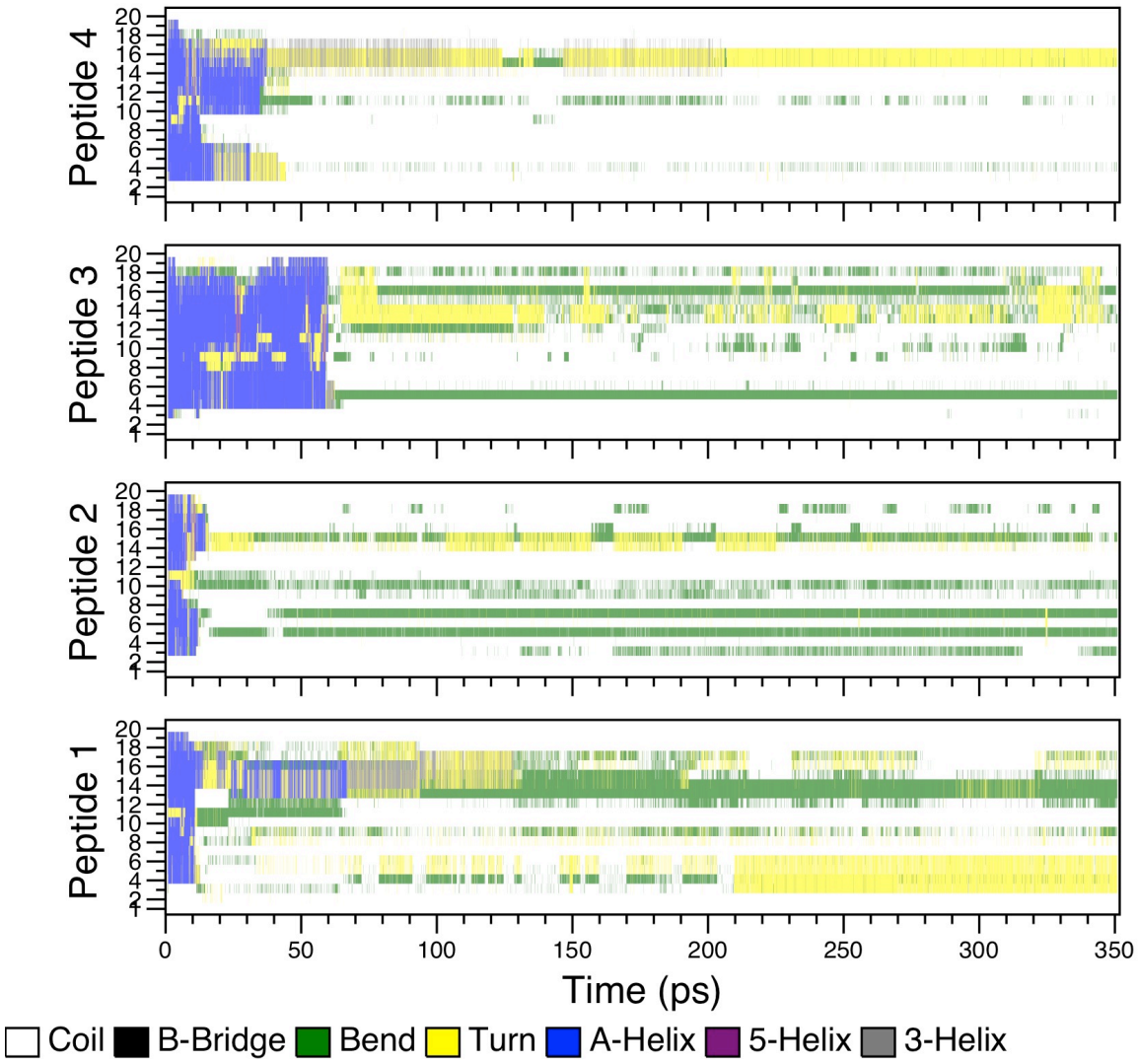

Figure S4. Secondary structure of the 4 peptides during the GNS simulation.

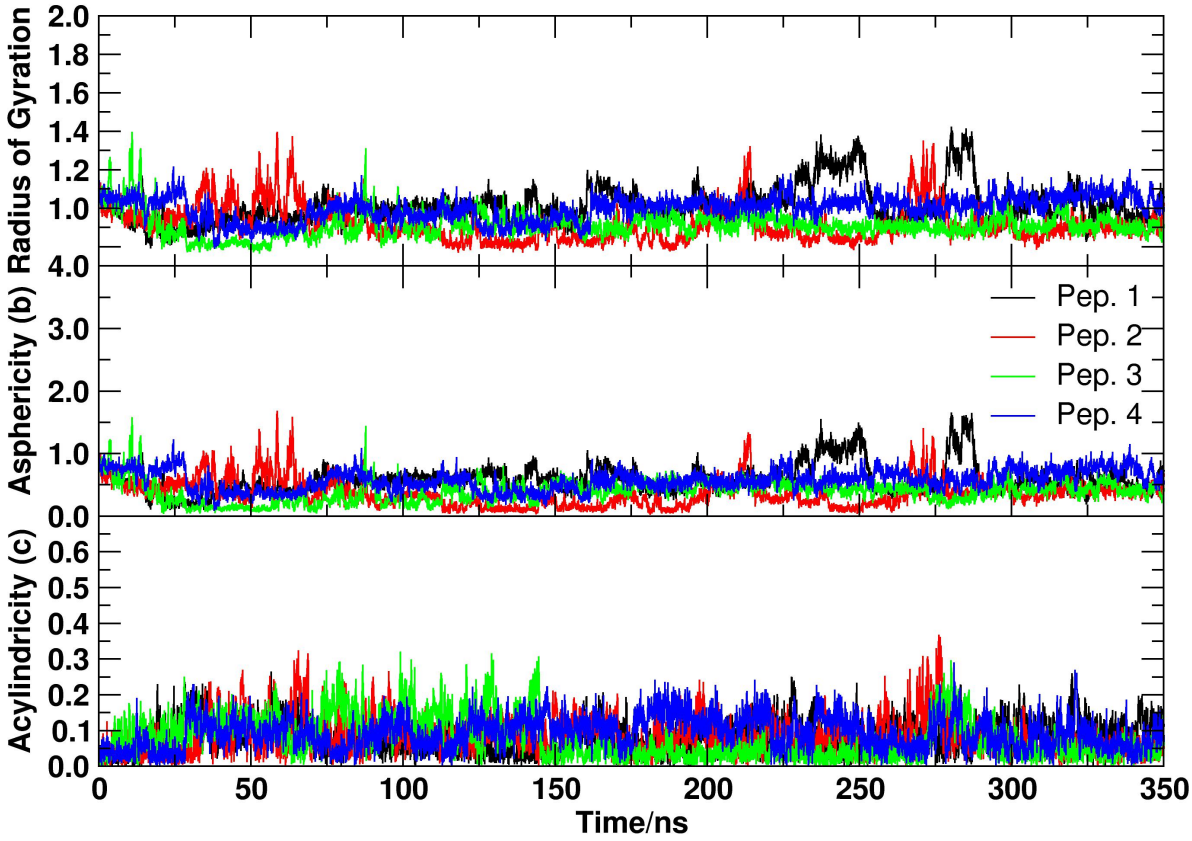

Figure S5. From top to bottom panel: radius of gyration (in nm), asphericity (in nm^2), and acylindricity (in nm^2) for the 4 peptides (different colored curves) in the pure water simulation. (Sarukhanyan, E.; Milano, G.; Roccatano, D. *Biopolymers* **2015**, *103*, 1).

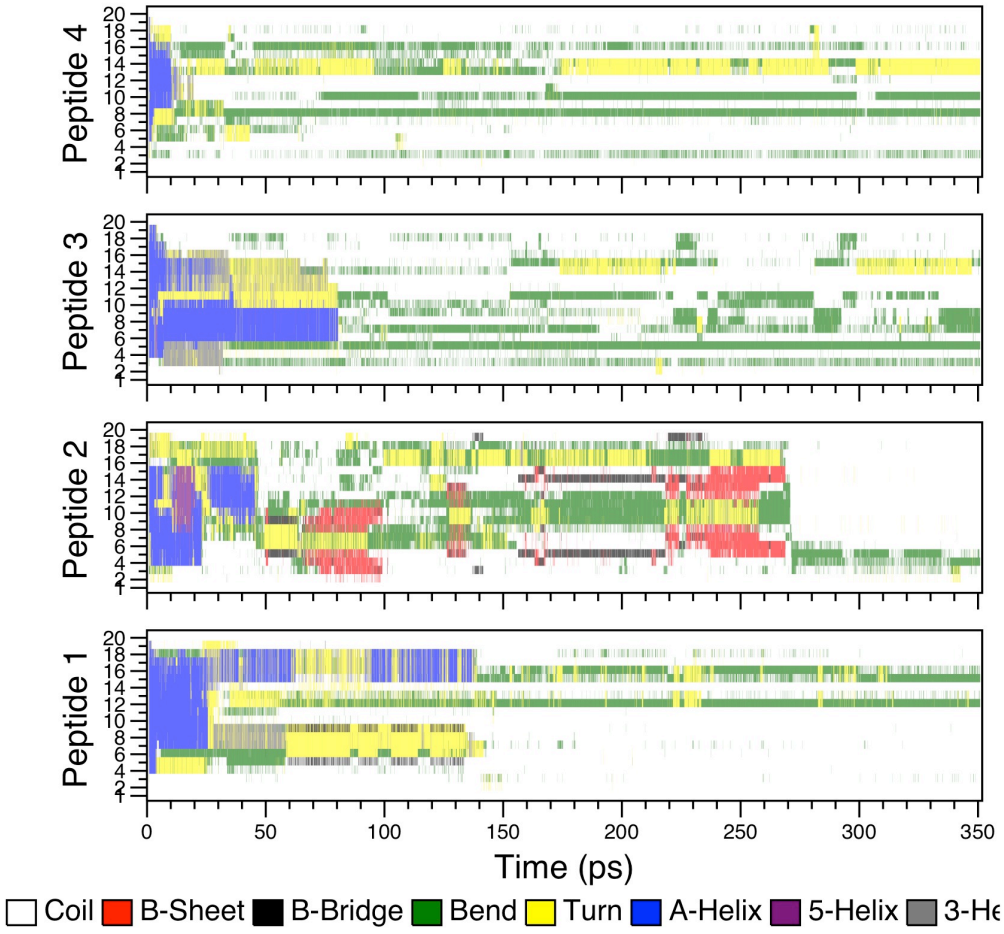

Figure S6. Secondary structure changes in the simulation of 4 CA-MA peptides with with the CNT.

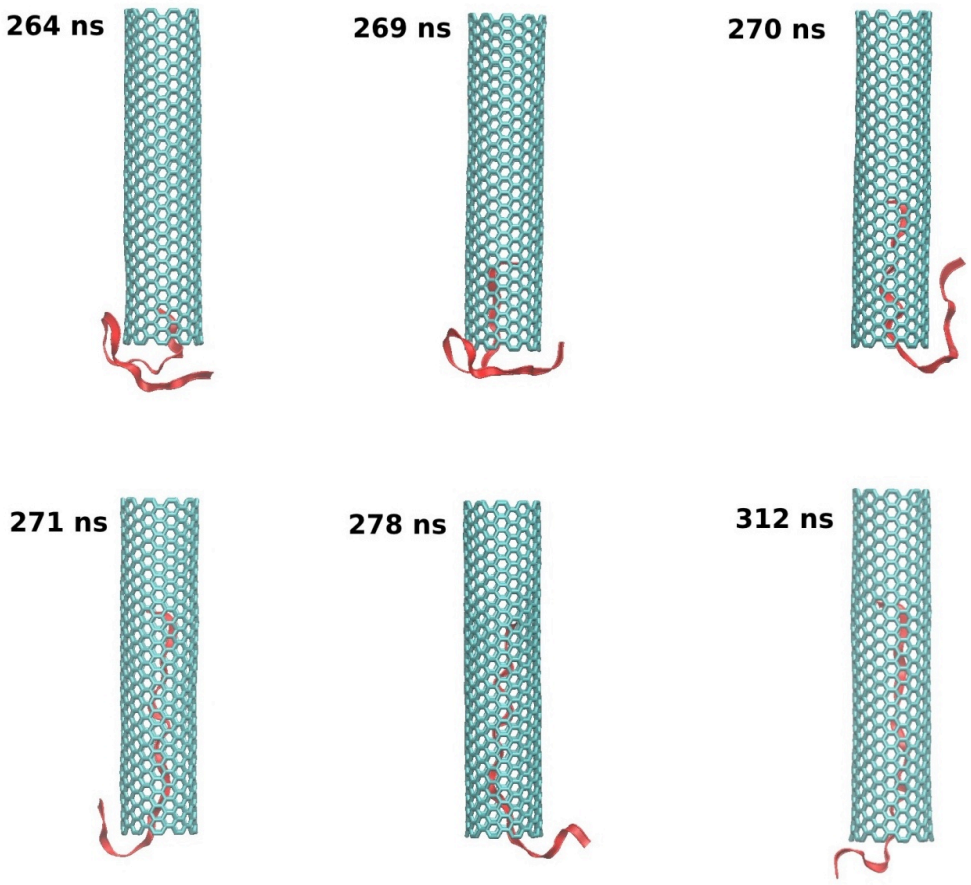

Figure S7. Snapshots from the simulation 4PC showing the event of spontaneous diffusion of peptide 2 inside the interior of the CNT.

.

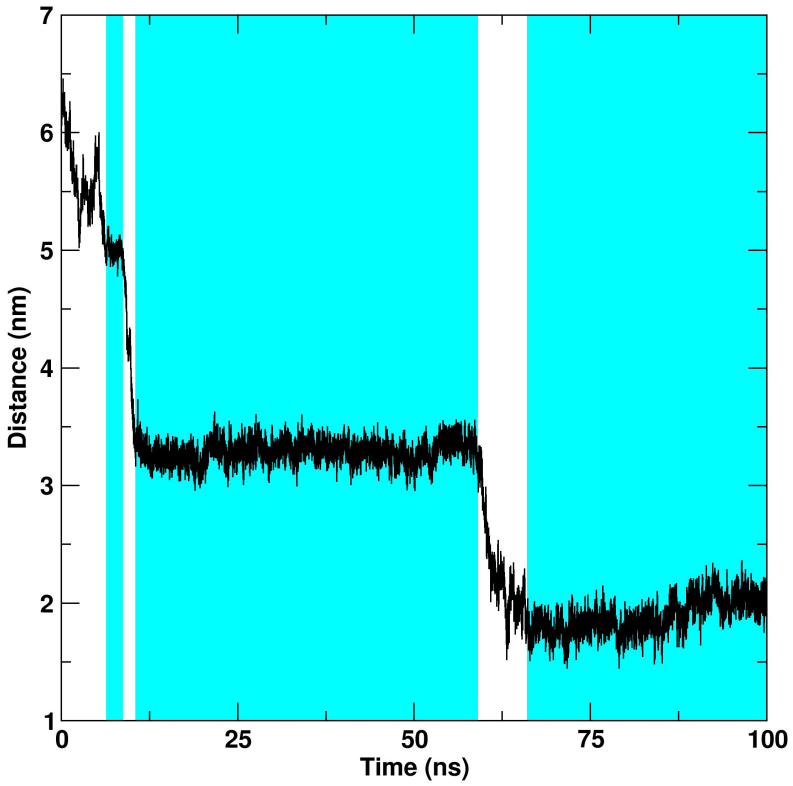
Distance (nm)
Time (ns)
1
2
3
4
5
6
7
0
25
50
75
100

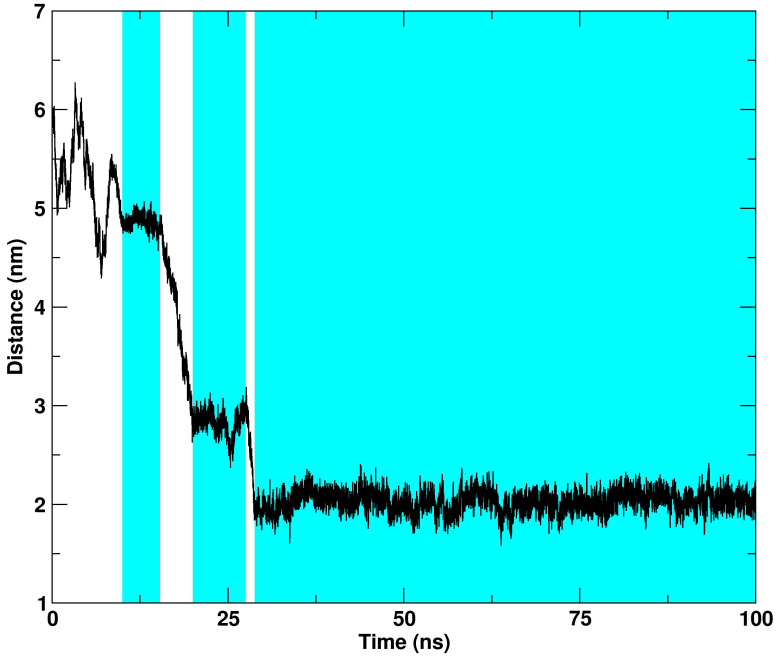
Distance (nm)
Time (ns)
1
2
3
4
5
6
7
0
25
50
75
100

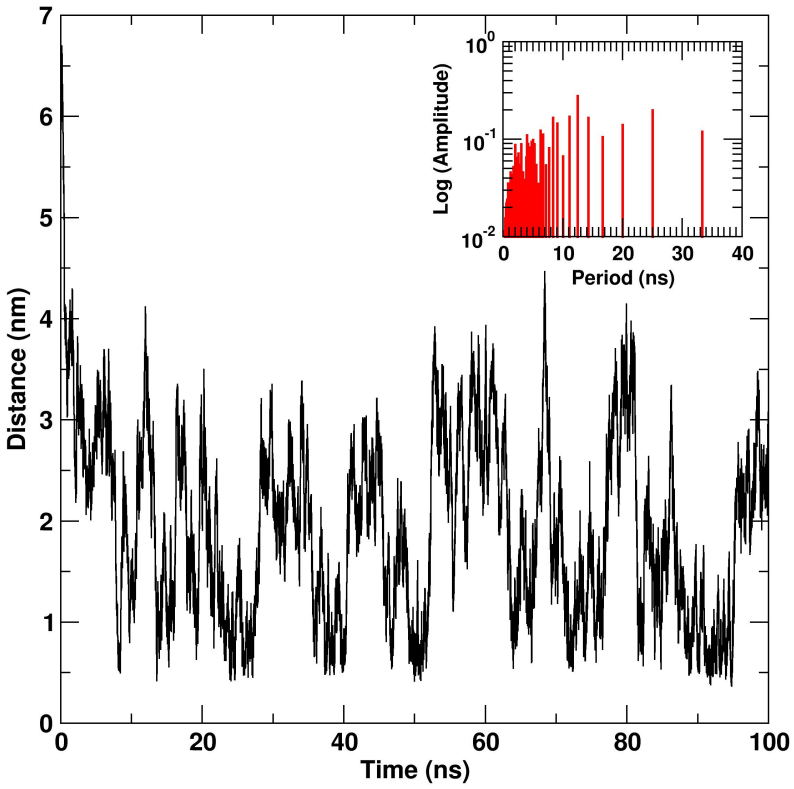

Figure S8. Graphs of the variations in time of the distance between the F20 (C-α atom) of the peptide and the carbon atoms on the rim of the SWCNT. Top: SWCNT with united atoms on the rim (1PC simulation). Middle: SWCNT with one-side fluorinated nanotube (1PCF simulation). Bottom: SWCNT with one-side protonated nanotube (1PCH simulation).

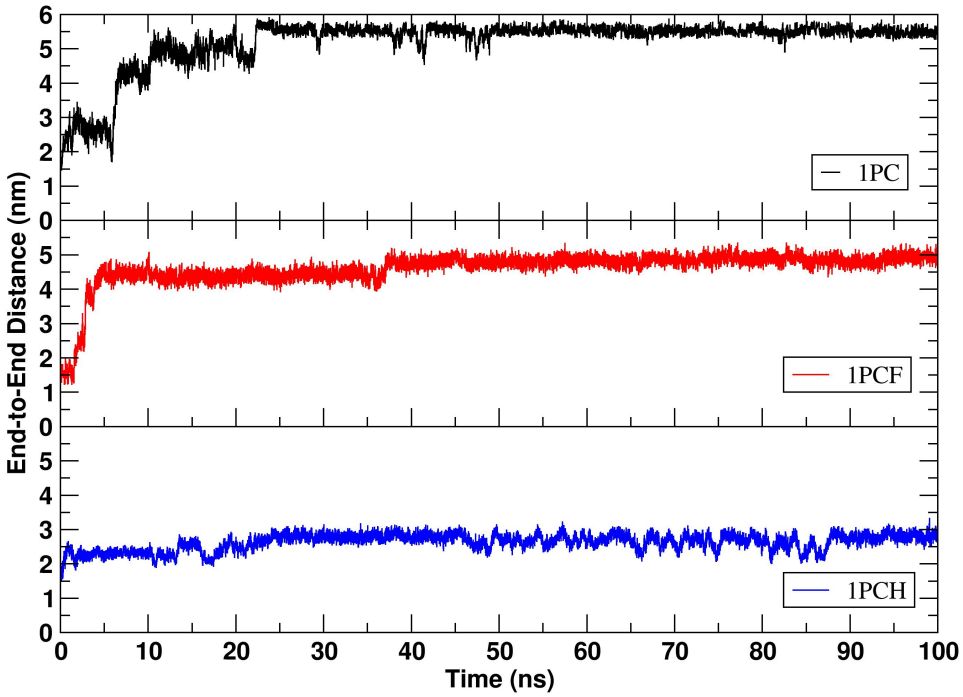

Figure S9. Time series of the distance between the Cα atoms of Lys1 and Phe20 of the peptide during the 1PC, 1PCF, 1PCH simulations.